Improved Description of Intra- and Intermolecular Interactions Through Dispersion-Corrected Second-Order Møller-Plesset Perturbation Theory

Gregory J. O. Beran,*,† Chandler Greenwell,† Cameron Cook,† and Jan Řezáč‡

†Department of Chemistry, University of California, Riverside, California 92521 USA ‡Institute of Organic Chemistry and Biochemistry, Czech Academy of Sciences, 166 10 Prague, Czech Republic

E-mail: gregory.beran@ucr.edu

Conspectus

The quantum chemical modeling of organic crystals and other molecular condensed-phase problems requires computationally-affordable electronic structure methods which can simultaneously describe intramolecular conformational energies and intermolecular interactions accurately. To achieve this, we have developed a spin-component-scaled, dispersion-corrected second-order Møller-Plesset perturbation theory (SCS-MP2D) model. SCS-MP2D augments canonical MP2 with a dispersion correction which removes the uncoupled Hartree-Fock dispersion energy present in canonical MP2 and replaces it with a more reliable coupled Kohn-Sham treatment, all evaluated within the framework of Grimme's D3 dispersion model. The spin-component scaling is then used to improve the description of the residual (nondispersion) portion of the correlation energy.

The SCS-MP2D model improves upon earlier corrected MP2 models in a few ways. Compared to the highly successful dispersion-corrected MP2C model, which is based solely on intermolecular perturbation theory, the SCS-MP2D dispersion correction improves the description of both inter- and intramolecular interactions. The dispersion correction can also be evaluated with trivial computational cost,

and nuclear analytic gradients are computed readily to enable geometry optimizations. In contrast to earlier spin-component scaling MP2 models, the optimal spin-component scaling coefficients are only mildly sensitive to the choice of training data, and a single global parameterization of the model can describe both thermochemistry and non-covalent interactions.

The resulting dispersion-corrected, spin-component-scaled MP2 (SCS-MP2D) model predicts conformational energies and intermolecular interactions with accuracy comparable to or better than that of many range-separated and double-hybrid density functionals, as is demonstrated on a variety of benchmark tests. Among the functionals considered here, only the revDSD-PBEP86-D3(BJ) functional gives consistently smaller errors in benchmark tests. The results presented also hint that further improvements of SCS-MP2D may be possible through a more robust fitting procedure for the seven empirical parameters.

To demonstrate the performance of SCS-MP2D further, several applications to molecular crystal problems are presented. The three chosen examples all represent cases where density-driven delocalization error causes GGA or hybrid density functionals to artificially stabilize crystals exhibiting more extended π -conjugation. Our pragmatic strategy addresses

the delocalization error by combining a periodic density functional theory (DFT) treatment of the infinite lattice with intramolecular/conformational energy corrections computed with SCS-MP2D. For the anti-cancer drug axitinib, applying the SCS-MP2D conformational energy correction produces crystal polymorph stabilities that are consistent with experiment, in contrast to earlier studies. For the crystal structure prediction of the ROY molecule, so named for its colorful red, orange, and vellow crystals, this approach leads to the first plausible crystal energy landscape, and it reveals that all of the lowest-energy polymorphs have already been found experimentally. Finally, in the context of photomechanical crystals, which transform light into mechanical work, these techniques are used to predict the structural transformations and extract design principles for maximizing the work performed.

Key References

- Greenwell, C; Řezáč, J.; Beran, G. J. O. "Spin-component-scaled and dispersion-corrected second-order Møller-Plesset perturbation theory: A path toward chemical accuracy." Phys. Chem. Chem. Phys. 2022, 24, 3695–3712. The SCS-MP2D model is developed and benchmarked on a variety of data sets and challenging examples.
- Greenwell, C; Beran, G. J. O. "Inaccurate conformational energies still hinder crystal structure prediction in flexible organic molecules." Cryst. Growth Des. 2020, 20, 4875–5881. The impact of DFT delocalization error on conformational polymorph energy rankings is demonstrated, along with how dispersion-corrected MP2 can be used to address the problem.
- Beran, G. J. O.; Sugden, I. J.; Greenwell,
 C; Bowskill, D H.; Pantelides, C. C.; Adjiman, C. S. "How many more polymorphs of ROY remain undiscovered?" Chem.

- Sci. 2022, 13, 1288–1297. Crystal structure prediction techniques combining periodic DFT and dispersion-corrected MP2 are used to investigate one of the most famous examples of polymorphism, the ROY molecule.
- Cook, C. J.; Li, W.; Lui, B. F.; Gately, T. J.; Al-Kaysi, R. O.; Mueller, L. J.; Bardeen, C. J.; Beran, G. J. O. "A theoretical framework for the design of molecular crystal engines." *Chem. Sci.* **2023**, 14, 937–949. A first-principles approach for predicting photomechanical responses in organic crystals is presented.

1 Introduction

As the least computationally-expensive correlated wave function method, second-order Møller-Plesset perturbation theory (MP2) has long held an important role in quantum chemistry. In recent decades, however, MP2 and other correlated wave function methods have largely been supplanted by density functional theory (DFT) for most practical applications of quantum chemistry, due to the good balance between accuracy and computational efficiency often provided by DFT functionals. Effective mathematical forms for hybrid, rangeseparated hybrid, and double-hybrid functionals, accurate and inexpensive models for London (a.k.a. van der Waals) dispersion, and improved data-driven parameterization strategies have all led to the development of robust functionals. 5-7

Still, computationally affordable alternatives to DFT remain valuable for situations where the behavior of DFT functionals proves problematic. The relatively low computational cost of MP2 makes it a logical alternative to DFT, but it exhibits mediocre performance on large benchmark data sets. This situation has motivated many efforts to improve MP2, including via spin-component scaling, ⁸ dispersion correction, ^{1,9-13} orbital optimization, ^{14,15} Coulomb attenuation, ^{16,17} regularization, ¹⁸ and the mixing in of contributions from third-order perturbation theory (e.g. MP2.5). ¹⁹

Motivated by our own research interests in organic molecular crystals, we have combined dispersion correction ¹³ and spin-component scaling, 1 to develop a robust MP2 model which describes non-covalent interactions with an accuracy and computational cost that avoids the density-driven delocalization error issues that plague many lower-rung density functionals and which is competitive with top-tier density functionals. In this research account, we briefly review the theory of SCS-MP2D, we demonstrate its performance relative to a selection of high-quality DFT functionals on benchmark data sets, and we discuss several applications to molecular crystals where the improved SCS-MP2D intramolecular/conformational energies proved crucial.

2 Dispersion-Corrected MP2

MP2 has a nominal advantage over widely-used semi-local density functionals in that it inherently includes London dispersion. Unfortunately, the MP2 dispersion treatment is often quantitatively inaccurate. For example, MP2 over-binds intermolecular π - π interactions by \sim 40% on average. ²⁰ To understand these errors, consider the dispersion energy term that occurs at second-order in intermolecular perturbation theory,

$$E_{disp}^{(2)} = -\sum_{m,n\neq 0} \frac{|\langle \phi_0^A \phi_0^B | \hat{V}^{AB} | \phi_m^A \phi_n^B \rangle|^2}{E_m^A - E_0^A + E_n^B - E_0^B}$$
 (1)

where ϕ_m^A and ϕ_n^B are the ground (m=0) and excited state wavefunctions on molecules A and B, and E_m^A and E_n^B are the ground and excited state energies of the two molecules.

The MP2 dispersion interactions are computed at the uncoupled Hartree-Fock (UCHF) level of theory. ^{21,22} This amounts to approximating the excited-state wavefunctions in Eq 1 by replacing occupied molecular orbitals in the ground state wavefunction with virtual ones (without any orbital relaxation), and approximating the excitation energies as the HF orbital energy differences between the pairs of orbitals being swapped. This simplified description pro-

duces the mediocre MP2 dispersion energies. More accurate dispersion energies can be obtained by modeling the excited states and excitation energies entering Eq 1 with either time-dependent HF (a.k.a. coupled HF, or CHF) or time-dependent DFT (a.k.a. coupled Kohn-Sham or CKS), both of which incorporate orbital relaxation and provide more reliable excitation energies.

In 2007, Cybulski and Lytle showed that MP2 could be improved by incorporating CHF dispersion. ²³ Shorty thereafter, Hesselmannn demonstrated an even more successful "corrected" MP2 (MP2C) model ^{9,10} which replaces the UCHF dispersion energy with the CKS one:

$$E_{MP2C} = E_{MP2} - E_{disp}^{UCHF} + E_{disp}^{CKS} \qquad (2)$$

MP2C performs excellently on a wide array of intermolecular interaction energy benchmarks, ²⁴ but it also has limitations. First, the computational cost of evaluating the dispersion correction is non-trivial. Second, its basis in intermolecular perturbation theory mean that MP2C cannot correct the intramolecular dispersion interactions which can become significant in larger molecules. Third, the complexity of the analytical nuclear gradients for the dispersion correction has hindered the use of MP2C for geometry optimizations.

To address these limitations, we proposed the dispersion-corrected MP2 (MP2D) model. ¹³ The MP2D energy expression is identical to Eq 2, except that the UCHF and CKS dispersion contributions are evaluated using a model based on Grimme's D3 dispersion approach, ²⁵

$$E_{disp} = -s_6 \sum_{a,b} f_6(R_{ab}) \frac{C_{6,ab}}{R_{ab}^6} - s_8 \sum_{a,b} f_8(R_{ab}) \frac{C_{8,ab}}{R_{ab}^6}$$
(3)

Here, R_{ab} is the distance between atoms a and b, C_6 and C_8 are interatomic two-body dispersion coefficients, and s_6 and s_8 are empirical scaling factors. The damping functions f_n attenuate the dispersion energy at short R_{ab} .

The D3 model stores a list of pre-computed dispersion coefficients for different elements computed from the frequency-dependent polarizabilities of the elemental hydrides (e.g. OH_x ,

for x = 0, 1, 2). When applying D3, the dispersion coefficient for a given atom is interpolated among those tabulated values based on the local coordination environment. MP2D uses the existing D3 dispersion coefficients for the CKS portion. ²⁵ New UCHF dispersion coefficients were computed for MP2D following the D3 protocols. ¹³ MP2D omits the Axilrod-Teller-Muto 3-body dispersion term that is sometimes included in D3, though it could potentially be helpful to include it in the future. ¹²

In total, MP2D has five global empirical parameters whose values were fitted to reproduce benchmark coupled cluster results from the S66x8 set of dimer interaction energies. HP2D is conceptually similar to the MP2+vDW method proposed earlier by Tkatchenko et al., 11 but the use of the D3 model in MP2D simplifies the process of obtaining the UCHF and CKS dispersion coefficients.

MP2D addresses the dispersion errors inherent in MP2, but there are other limitations of second-order perturbation theory. MP2 overestimates the same-spin electron-electron correlation often associated with static correlation relative to the opposite-spin contributions which are more associated with dynamical correlation. ²⁷ Grimme's spin-component-scaled MP2 (SCS-MP2)⁸ re-weights the two correlation energy components using empirical coefficients c_{ss} and c_{os} ,

$$E_{SCS-MP2} = E_{HF} + c_{os}E_{corr,os} + c_{ss}E_{corr,ss}$$
(4)

Spin-component scaling improves the performance of MP2, but the optimal empirical coefficients vary significantly depending on the training data. Notably, the optimal scaling parameters for non-covalent interactions²⁸ are almost reversed from those fitted to thermochemical reaction energies.⁸

The problem lies in how spin-component scaling is used to correct both the London dispersion and other non-dispersion aspects of the correlation energy, and the relative importance of these contributions is system-dependent. However, since MP2D addresses the dispersion treatment, spin-component scaling can be employed to correct only the residual correlation

energy. The combined SCS-MP2D energy expression subtracts out the dispersion energy component from the same- and opposite spin correlation energies, scales the residual correlation with empirical coefficients c_{os} and c_{ss} , and then adds the CKS dispersion:¹

$$E_{SCS-MP2D} = E_{HF} + c_{os} \left(E_{corr,os} - E_{disp,os}^{UCHF} \right) + c_{ss} \left(E_{corr,ss} - E_{disp,ss}^{UCHF} \right) + E_{disp,tot}^{CKS}$$
(5)

The seven empirical parameters in SCS-MP2D were fitted against the S66x8 set of dimer intermolecular interactions, sugar conformational energies (SCONF), and Diels-Alder reaction thermochemistry (DARC). The fitted values proved only mildly sensitive to the choice of training data used to fit them. To-date, the MP2D and SCS-MP2D dispersion coefficients have been determined for the elements H, B-Ne, P-Ar, and Br. MP2D is implemented in PSI4, ²⁹ as a stand-alone open-source library ³⁰ and in the Cuby4 framework ³¹ where the correction can be added to calculations in other software packages.

SCS-MP2D shares conceptual similarities with the dispersion-corrected, spin-componentscaled double hybrid (DSD) family of functionals. 7,32 Both employ Grimme-style dispersion corrections, spin-component scaling of the MP2-like correlation, and a large fraction of exact exchange (100% for SCS-MP2D and $\sim 70\%$ in the DSD functionals). However, the DSD functional mixes in semi-local exchangecorrelation and computes the MP2-like correlation in Kohn-Sham orbitals instead of HF ones, 33 while SCS-MP2D removes the MP2 UCHF dispersion contribution to avoid doublecounting of dispersion energy. Benchmark performance comparisons between the two types of models will be discussed below.

The computational cost of the MP2D models is effectively identical to that of MP2. For a chosen basis set, the cost is essentially the same as the DSD-family of double-hybrid functionals. Although the $O(N^5)$ scaling of these methods with system size N makes them formally more expensive than ω B97M-V, the large

pre-factor makes $\omega B97M\text{-V}$ noticeably slower even for fairly large molecules. For example, MP2D is $\sim\!40\%$ faster than $\omega B97M\text{-V}$ for drug molecule ritonavir (C₃₇H₄₈N₆O₅S₂, 98 atoms) in aug-cc-pVQZ. The accuracy of MP2D and SCS-MP2D will be discussed in the following sections.

3 Benchmark Calculations

All results presented below either use a quadruple- ζ basis set or have been extrapolated to the complete-basis-set limit. See the original studies for further computational details.

3.1 Conformational Energies

Initial conformational energy benchmarks for the dispersion-corrected MP2 models focused on existing test sets of sugar (SCONF), alkane (ACONF), amino acid (Amino20x4), peptide (PCONF21), and melatonin (MCONF) conformations. As shown in Table 1, applying the dispersion correction and spin-component scaling to MP2 reduces the root-mean-square errors (RMSEs) errors by 60% on average. The mean relative SCS-MP2D conformational energy error of 8.7% is on par with or smaller than those from DSD-BLYP-D3(BJ) (11.5%), ω B97X-V (8.9%), and ω B97M-V (14.1%). Only revDSD-PBEP86-D3(BJ) performs slightly better, with a mean relative error of 8.1%.

Predicting conformational energies accurately is key to understanding the interplay of intraand intermolecular interactions that drives the crystal packing. Therefore, a subsequent benchmark study examined 54 intramolecular conformations extracted from the conformational crystal polymorphs of 20 species that range from small organics to large drugs such as ritonavir. Intramolecular dispersion contributes significantly to many conformational energies in the test set, and adding the MP2D dispersion correction reduces the RMSE from 3.5 kJ/mol to 2.5 kJ/mol. SCS-MP2D further reduces the error to 1.9 kJ/mol.

Figure 1 plots the error distributions for SCS-MP2D and six DFT functionals relative to the

benchmark conformational energies. For 14 of the species, all models perform fairly well, with RMSE of 1.7–2..5 kJ/mol for the DFT functionals and 1.2 kJ/mol for SCS-MP2D. However, the remaining six species indicated in Figure 1 prove more problematic for the GGA and hybrid functionals, with errors \sim 2–4 times larger than those from ω B97M-V and SCS-MP2D.

Those difficulties stem from density-driven DFT delocalization error (sometimes called many-electron self-interaction error), which is the tendency of approximate density functionals to overly-delocalize electron densities. In the current context, the different crystal conformations of those six problematic species vary in the extent of π delocalization, ³⁶ and delocalization error artificially stabilizes the conformations exhibiting more π -conjugation (greater delocalization). In the species with Cambridge Structure Database reference codes MCHTEP, MNIAAN, and ACBNZA, for example, the extent of π -conjugation is controlled by the sidechain orientations (Figure 1). Delocalization error is pronounced in GGA functionals such as B86bPBE-XDM and PBE, and they exhibit the largest conformational energy errors for these species. The inclusion of 25% exact exchange in the hybrid PBE0 functional reduces the selfinteraction/delocalization error and moderately improves the conformational energies, though the PBE0 errors remain considerably larger than those from $\omega B97M-V$ or SCS-MP2D.

Overall, SCS-MP2D gives the smallest RMSE of 1.9 kJ/mol for the entire set of 20 species, compared to 2.3 kJ/mol with ω B97M-V and larger errors for the other models. Additional examples of using SCS-MP2D to address delocalization error will be presented in the molecular crystal applications below.

3.2 Intermolecular Interactions

Initial assessment¹ of the MP2D models for intermolecular interactions was carried out on several dimer data sets. As summarized in Table 1, the MP2D dispersion correction reduces the RMSEs for the intermolecular interaction data sets by up to several-fold, and spin-component scaling further reduces the errors

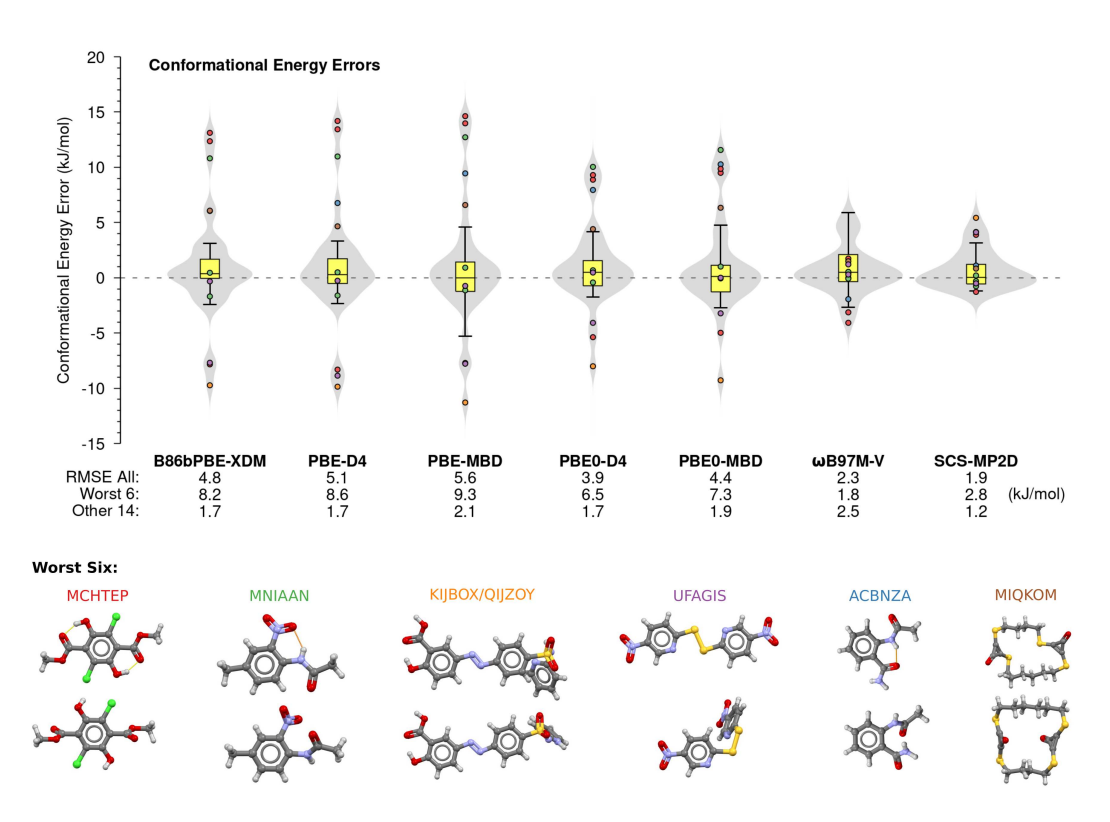


Figure 1: Error distributions for 54 molecular conformations extracted from conformational crystal polymorphs of 20 organic species. The overall error distribution is shown in gray, the errors for the six most problematic species are shown as points, and the box-and-whisker plots indicate the error distributions for the remaining 14 species. RMSEs for the three groups and representative conformations of the problematic species are shown below. Adapted with permission from ref. 36. Copyright 2022 AIP Publishing.

Table 1: Root-mean-square errors (kJ/mol) for several MP2 models and DFT functionals on benchmark data sets.^a

				DSD-	revDSD-		
Data Set	MP2	MP2D	SCS-MP2D	BLYP-D3(BJ)	PBEP86-D3(BJ)	$\omega \mathrm{B}97\mathrm{X}\text{-}\mathrm{V}$	$\omega \mathrm{B97M-V}$
	CBS	CBS	CBS	def2-QZVP	def2-QZVP	def2-QZVP	aQZ
Intermolecular Interactions							
S66x8	2.80	0.67	0.54^{b}	0.75	0.67	0.88	0.46
3B-69 Dimers	1.38	0.88	0.75	0.79	0.79	0.84	0.71
SSI	1.51	0.67	0.71	0.63^{c}	0.50	0.67^{d}	0.63^{d}
HBC6	1.34	1.09	1.05	1.55	0.71	1.34	1.00
NBC10	6.49	1.21	0.59	1.38	0.29	1.42	0.71
Charge Transfer	11.4	2.34	1.42	3.22	2.59	2.38	1.88
HB375	1.80	0.67	0.54	0.59	0.54	0.71	0.79
IHB100	1.88	1.92	1.42	1.72^{c}	1.09^{c}	1.55^{c}	1.46
Conformational Energies							
SCONF	1.30	1.46	0.75^{b}	1.09	0.54	0.88^{e}	1.00
ACONF	0.46	0.29	0.50	0.33	1.00	0.25^{e}	0.33
Amino20x4	1.09	0.71	0.75	0.67	0.71	1.00^{e}	1.00
MCONF	4.27	1.67	1.38	2.30	0.79	1.13^{e}	1.63
PCONF21	4.64	1.76	1.30	2.01	0.96	1.46^{e}	2.89
Reaction Energies							
DARC	16.6	7.95	5.90^{b}	4.60	2.68	18.3^{e}	4.10
ISO34	7.03	5.94	4.02	4.44	2.05	6.53^{e}	3.43
ISOL24	15.6	11.8	9.37	11.3	7.24	17.6^{e}	10.1
IDISP	29.4	5.94	5.40	6.69	2.80	16.2^{e}	11.8
Overall Relative RMSE Statistics							
Mean	21.3%	7.7%	5.9%	8.1%	4.9%	9.5%	8.2%
Median	11.5%	5.8%	4.4%	5.5%	4.1%	5.3%	4.5%

^a Adapted with permission from ref. 1. Copyright 2022 Royal Society of Chemistry.

by up to a third. The final SCS-MP2D errors for these sets are often smaller than those from DSD-BLYP-D3(BJ) and ω B97X-V, and they are competitive with ω B97M-V. In contrast, revDSD-PBEP86-D3(BJ) generally has even smaller errors than SCS-MP2D, with the exception of the charge-transfer complex data set.

For further insight, we present new benchmark results for five large data sets from the Non-Covalent Interactions Atlas (NCIAtlas): HNCO-containing hydrogen-bonded dimers (HB375x10), 37 hydrogen-bonded dimers involving S, P, and halogens (HB300SPXx10), 38 repulsive contacts (R739x10), 39 σ -hole interactions (SH250x10), 40 and dispersion-bound complexes (D442x10). 20 Species containing As, Se, Kr, I and Xe were omitted here (22% of the data set), since the necessary MP2 dispersion coefficients have not yet been determined.

Figure 2 plots the RMSEs for each NCIAtlas data set and indicates the average RMSE over all five data sets, comparing the MP2 models against several good-quality density functionals from the original studies. MP2 gives a poor av-

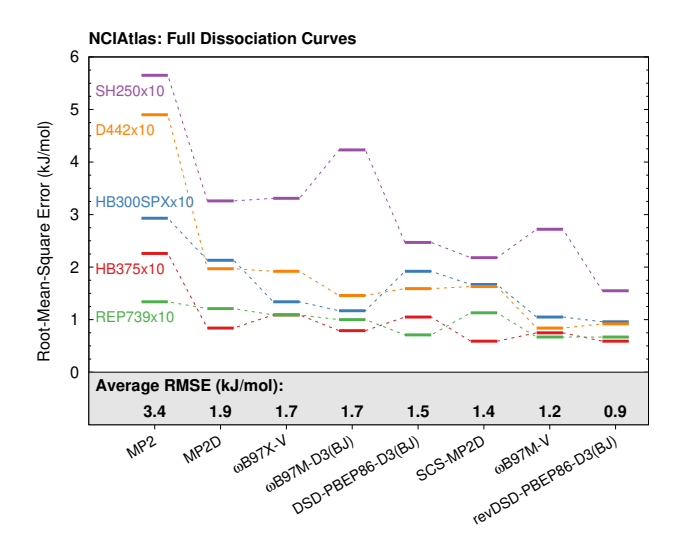


Figure 2: Performance of MP2 models and several top-performing density functionals on the NCIAtlas data sets.

^b Data sets used to fit SCS-MP2D parameters.

^c aug-cc-pVQZ basis

 $[^]d$ Ref 34, aug-cc-pVTZ basis.

 $[^]e$ Ref 35.

erage RMSE of 3.4 kJ/mol, but including the MP2D dispersion correction reduces the average error to 1.9 kJ/mol, and spin-component scaling further reduces it to 1.4 kJ/mol. This error is a little smaller than that of ω B97X-V or ω B97X-D3(BJ), and comparable to the original DSD-PBEP86-D3(BJ). On the other hand, ω B97M-V and revDSD-PBEP86-D3(BJ) give smaller average RMSEs of 1.2 and 0.9 kJ/mol, respectively.

Several features of the data stand out. First, the similar performance of SCS-MP2D and DSD-PBEP86-D3(BJ) functional is noteworthy because the empirical parameters in both models were fitted against modest amounts of training data. Refitting DSD-PBEP86-D3(BJ) against a much larger data set leads to the excellent performance observed for revDSD-PBEP86-D3(BJ). 7,32 We also observe that MP2D and SCS-MP2D perform better for HB375x10 than for HB300SPXx10. The latter set includes chemical elements that were not present in the (SCS-)MP2D training data, perhaps further indicating a limitation of the training data used. These results raise the question: might a more robust parameter fitting procedure improve SCS-MP2D similarly to what was found with revDSD-PBEP86-D3(BJ)?

Second, the MP2 model errors for the repulsive contacts (REP739x10) are consistently larger than those from the DFT functionals, suggesting that efforts to improve the shortrange performance of SCS-MP2D would be helpful. Third, the SCS-MP2D RMSE on the D442x10 dispersion-bound complexes is similar to that of $\omega B97M-D3(BJ)$ and somewhat larger than for $\omega B97M-V$. This could suggest that the approximations inherent in the D3 dispersion correction may limit the accuracy of SCS-MP2D somewhat (though revDSD-PBEP86-D3(BJ) performs very well with D3). Fourth, SCS-MP2D has comparatively small errors for the σ -hole interactions, with only revDSD-PBEP86-D3(BJ) performing better.

Additional benchmark MP2D and SCS-MP2D calculations for intermolecular interactions can be found in refs 36 and 41.

3.3 Reaction Thermochemistry

To date, MP2D and SCS-MP2D have only been benchmarked on a handful of thermochemistry data sets. 1 As shown in Table 1, the MP2D dispersion correction only modestly impacts the accuracy of small-molecule ISO34 isomerization energies, but it improves the largermolecule isomerizations of ISOL24 more significantly. The effects on the Diels-Alder reactions (DARC) and the intramolecular dispersion (IDISP) set, which includes some challenging reaction energies, are even larger. Spincomponent scaling of MP2D further reduces the errors by $\sim 10-30\%$. In the end, the SCS-MP2D errors for these data sets are mostly smaller than the range-separated hybrid $\omega B97X-V$ or early-generation DSD-BLYP-D3(BJ) functionals. The comparison between $\omega B97M-V$ and SCS-MP2D is more mixed, while the revDSD-PBEP86-D3(BJ) functional consistently performs the best.

In summary, SCS-MP2D describes intra- and intermolecular interactions with an accuracy that is competitive with some of the very best density functionals. More extensive investigations will be needed to fully assess the performance of SCS-MP2D for reaction thermochemistry. The greater tendency for spin-contamination in HF orbitals compared to Kohn-Sham ones might prove problematic for SCS-MP2D barrier heights and open-shell species, though the use of a restricted open-shell HF reference ³³ or orbital optimization ^{14,15} might mitigate the issue.

4 Applications to Molecular Crystals

Having examined the performance of the improved MP2 methods, we now focus on molecular crystal applications. Direct application of MP2 to molecular crystals via periodic boundary conditions is computationally expensive. Fragment methods based on the many-body expansion, 42 such as our hybrid many-body interaction approach, 43 can be used to lower the cost. For example, we have applied fragment-

based MP2 to molecular crystals to examine the polymorphism of aspirin⁴⁴ and oxalyl dihydrazide, ⁴⁵ to predict the polymorph phase diagram of methanol, ⁴⁶ and to investigate high-pressure phases of several species. ^{47–50} Further examples from Hirata⁵¹ and Červinka^{52,53} can also be found in the literature.

In analyzing the behavior of MP2 and DFT on challenging examples of conformational polymorphism, ^{36,41} we found a number of systems for which the intramolecular GGA or hybrid DFT conformational energies were problematic due to delocalization error, while the intermolecular interactions were described reasonably well. This motivated the development of a computationally pragmatic approach which describes intermolecular interactions with periodic DFT, while intramolecular ones are modeled using a higher level of theory such as SCS-MP2D.²

Specifically, the crystal energy is evaluated by performing the periodic DFT calculation, subtracting out the gas-phase DFT energy of each individual molecule in the unit cell, and replacing those energies with the gas-phase SCS-MP2D energy:

$$\tilde{E} = E_{crystal}^{DFT} + \sum_{i} \left(E_{molec,i}^{SCS-MP2D} - E_{molec,i}^{DFT} \right)$$
 (6)

The gas-phase correction typically only needs to be evaluated for 1–2 symmetrically-unique molecules in the unit cell, and the added computational cost of the energy correction is modest compared to periodic DFT. We now discuss several examples where this combination of periodic DFT and SCS-MP2D proved useful. Additional examples can be found in the literature. ^{2,36,54} In these examples, Eq 6 was applied as a single-point energy correction to crystal structures optimized with B86bPBE-XDM. The combination of B86bPBE-XDM and SCS-MP2D energies has proved effective in benchmarks³⁶ and applications, ^{2,3} though one could potentially employ other density functionals instead of B86bPBE-XDM. One might also wish to use the SCS-MP2D correction to refine the crystal geometries, though this has not been investigated for reasons of computational expedience.

4.1 Axitinib

Pfizer's kinase inhibitor axitinib has five known polymorphs (forms I, IV, VI, XXV, and XLI), and 66 solvates. 55,56 Forms XXV and XLI were discovered serendipitously during the late stages of drug formulation, and the thermodynamically most stable form XLI was eventually used in the commercial formulation. Crystal structure prediction could plausibly have helped discover these two polymorphs sooner, streamlining the drug's development. sequent crystal structure prediction studies did indeed generate these experimental polymorphs, though the energy rankings were poor and inconsistent with experiment when a forcefield, ⁵⁷ mixed force-field/DFT energy model, ⁵⁸ or periodic GGA DFT² were used. GGA functional B86bPBE-XDM erroneously predicts forms VI and XXV to be more stable than form XLI (Figure 3b), for example.

The incorrect GGA energy rankings stem primarily from poor intramolecular conformational energies.² Axitinib adopts an extended conformation in most polymorphs. However, in form XLI, the molecule folds to create a π - π interaction between the amide and indazole ring, disrupting the π -conjugation between the amide and benzene ring. DFT delocalization error artificially destabilizes the form XLI conformation relative to the extended conformations which exhibit more π -conjugation. In Figure 3a, comparing PBE-D3(BJ) against the DLPNO-CCSD(T1) benchmarks reveals the over-stabilization of several molecular conformations relative to form XLI, with a net RMSE of 4.0 kJ/mol. Switching to the global hybrid PBE0-D3(BJ) partially corrects the conformational energies, but the RMSE remains 1.5 kJ/mol.The range-separated $\omega B97M-V$ appears to over-compensate, stabilizing form XLI too much and giving a worse RMSE of 2.7 kJ/mol. In contrast, MP2D, SCS-MP2D, and DSD-PBEP86-D3(BJ) perform much better, with RMSEs of 0.5 kJ/mol relative to the coupled cluster benchmarks, while revDSD-PBEP86-D3(BJ) gives a slightly smaller RMSE

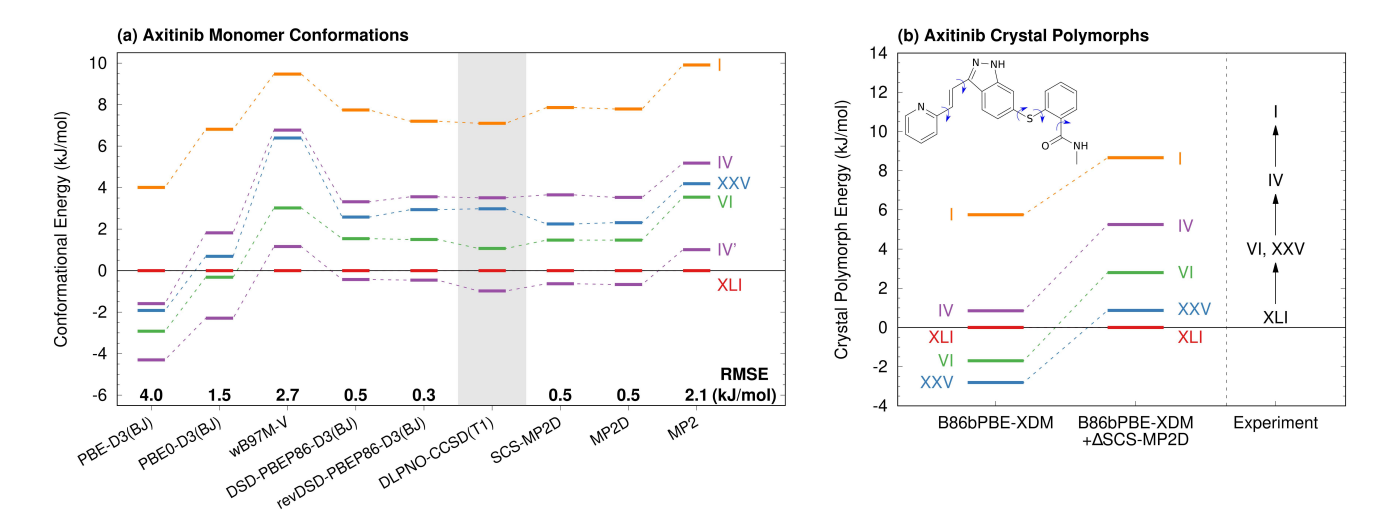


Figure 3: (a) Conformational energies for the six symmetrically unique conformations found in the experimental polymorphs of axitinib. RMSEs for each model are indicated in bold (kJ/mol). (b) The SCS-MP2D monomer correction brings the B86bPBE-XDM polymorph energies into qualitative agreement with experimental enthalpic stabilities.

of 0.3 kJ/mol. Intramolecular dispersion is quite important in this system, and the MP2 errors are four times larger than MP2D or SCS-MP2D.

Figure 3b highlights how applying an SCS-MP2D intramolecular conformational energy correction to periodic B86bPBE-XDM leads to relative 0 K lattice energies that are consistent with experimental finite-temperature enthalpies (note there is some ambiguity regarding the experimental ordering of forms VI and XXV).²

4.2 ROY

Consider next the ROY molecule, so named for its brilliant red, orange, and yellow crystals. This prolific polymorph former holds a record of 12 fully characterized crystal forms reported to-date ^{59,60} along with at least one incompletely characterized form. ⁶¹ Crystal structure prediction techniques successfully generate all of these polymorphs, ^{61,62} and some polymorphs were even predicted before they were discovered experimentally. ⁶³ However, the ROY polymorph energy rankings based on force fields, GGAs, or hybrid DFT disagree strongly with experiment. Most dramatically, form Y is the most stable polymorph experimentally, but multiple GGA and hybrid DFT functionals predict it to

be one of the least stable among the experimental forms.^{2,64}

To address this problem, we undertook a new crystal structure prediction study (Figure 4).³ Once again, the key difficulty lies in the ROY conformational energies. The polymorph colors stem largely from different conformations of the ROY molecule that vary the extent of π-conjugation between the two aromatic rings.⁶⁵ Conventional GGA and hybrid functionals over-stabilize the more planar conformations found in red and orange polymorphs relative to the nearly perpendicular yellow conformation (Figure 4a).^{2,41,61,66} Models such as SCS-MP2D or revDSD-PBEP86-D3(BJ) produce conformational energy curves that are much closer to CCSD(T) benchmarks.¹

As shown in Figure 4b, B86bPBE-XDM predicts the red and orange polymorphs (R, R18, R05, ON, OP, etc) to be more stable than the yellow ones (Y, YN, YT04, etc). Applying an intramolecular conformational energy correction with MP2D or SCS-MP2D reorders the polymorph stabilities and significantly improves the agreement with experiment (Figure 4c). ^{2,3,41} Among the seven polymorph whose stabilities are well-known experimentally, ⁵⁹ the SCS-MP2D-corrected landscape ranks all but YN and ON correctly, and those two are reversed by less than 1

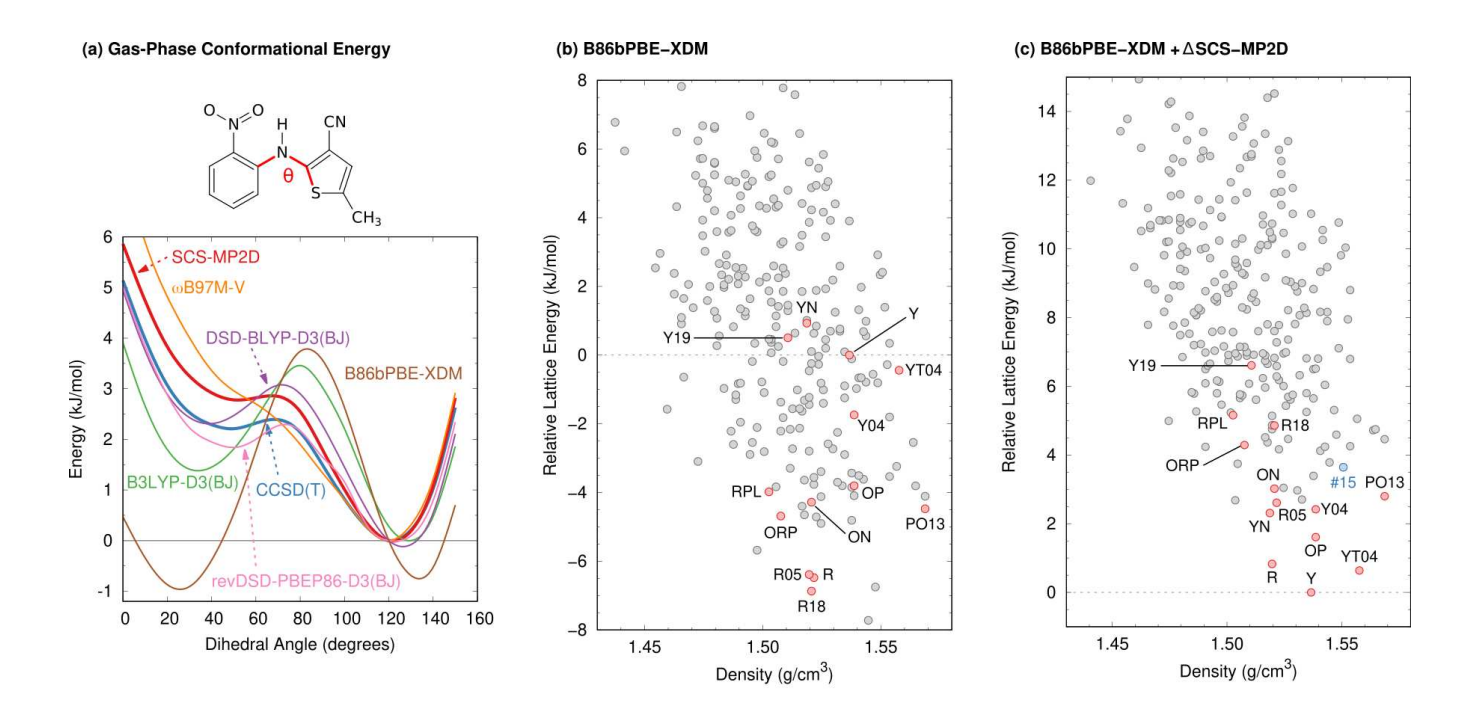


Figure 4: (a) Gas-phase conformational energy scan for the ROY molecule about the indicated angle θ . Crystal energy landscapes for ROY as computed with (b) B86bPBE-XDM and (c) after applying the intramolecular SCS-MP2D correction. Each point represents a crystal structure. Adapted from ref. 3. Copyright 2022 the authors. Published by Royal Society of Chemistry under a CC BY 3.0 DEED Attribution 3.0 Unported License.

kJ/mol. Applying the SCS-MP2D correction to B86bPBE-XDM lattice energies reduces the RMSE versus relative experimental enthalpies from 6.1 kJ/mol to just 0.4 kJ/mol, even if the the neglect of finite temperature vibrational contributions in the calculations makes this agreement partly fortuitous.³

The final landscape in Figure 4c shows that nine of the twelve most stable polymorphs have already been discovered experimentally. Moreover, the four forms predicted to be the least stable (ORP, R18, RPL, and Y19) are all known to be metastable or they required unusual conditions to crystallize, which is consistent with their higher energies. While one can never entirely rule out the experimental discovery of new polymorphs, the landscape in Figure 4c suggests that the most stable crystal forms have already been found, and that producing new forms will likely require serendipity or specialized crystallization strategies that can trap metastable forms. Among the hypothetical

crystal forms on the landscape, the rank 15 structure stands out because it is predicted to become more stable than all other forms near pressures of 10 GPa.³ It remains to be seen whether this putative high-pressure polymorph can be obtained experimentally.

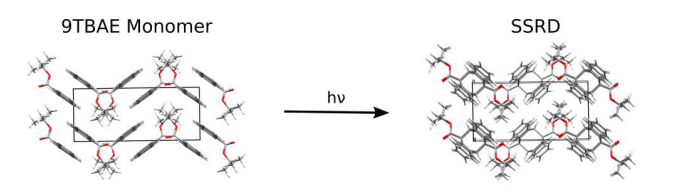
4.3 Photomechanical Crystals

Finally, consider a series of photomechanical molecular crystals based on anthracene derivatives. Anthracenes can undergo a solid-state [4+4] photodimerization under UV irradiation. If performed in a micro- or nanoscale crystal, the photochemical reaction induces a crystal-to-crystal transformation that deforms the material. ⁶⁷ For example, nanorods of 9-tert-butyl anthracene ester (9TBAE) irreversibly elongate by 8%, ⁶⁸ while microribbons of 9-anthracene carboxylic acid (9AC) twist, only to revert back to their original state thermally on a time scale of minutes. ⁶⁹ The deformations occurring

in photomechanical crystals can produce exceptional work densities. Unfortunately, understanding the atomistic details of the crystal transformation and how to engineer desired photomechanical response properties has proved difficult experimentally, and work todate has largely been performed on a trial-anderror basis. ⁶⁷

After initial collaborative efforts combining theory and experiment to understand selected crystal structure transformations ^{68,70} and energetics, ^{71,72} we have now developed a general approach for predicting these photomechanical transformations in these materials entirely in silico. 4 Starting from the crystal structure of the reactant (obtained either from experiment or crystal structure prediction), we predict the topochemical solid-state transformation. Using the stress and strain tensors associated with the deformation, we have found that these photomechanical crystals can potentially produce massive work densities up to $\sim 10^7 - 10^8$ J/m³. ^{4,73,74} By relating the changes in molecular structure to the anisotropic solid-state response, we have elucidated the design principles which emphasize the crystal engineering of parallel photochrome packing motifs to maximize the anisotropic response, 73 and we have explored the impacts of making minor chemical modifications (e.g. halogenation) to the photochrome. 74

During the course of these studies, however, the difficulty arose that density-driven delocalization error causes common GGA and hybrid density functionals to artificially destabilize the photodimer product by $\sim 60-75$ kJ/mol relative to the reactants. 4,71,74,75 In contrast, SCS-MP2D reproduces CCSD(T) benchmark energies for the photodimer to within 5 kJ/mol.¹ Figure 5 shows the impact of addressing the DFT errors on the ideal photomechanical engine cycle used to assess thermodynamics and work associated with these photomechanical transformations. This cycle starts with the monomer crystal, photodimerizes the molecules within the monomer unit cell (red) to form the proto-solid-state reacted dimer (proto-SSRD), and then relaxes the SSRD to its equilibrium crystal structure (blue). This relaxation re-



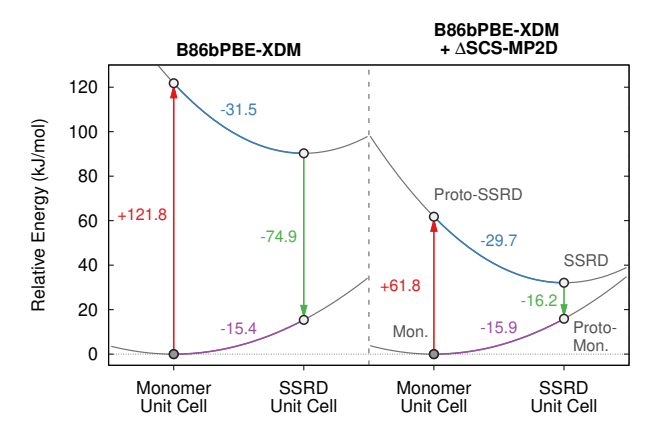


Figure 5: Photodimerization of 9TBAE monomer reactant crystal to the solid-state reacted dimer (SSRD) product, and schematic energy diagrams for the associated thermodynamic cycle before and after applying an intramolecular SCS-MP2D correction to the periodic B86bPBE-XDM energies.

leases stress and deforms the crystal, thereby performing the forward-stroke work. The reverse direction dissociates the SSRD back to the monomer (green) and relaxes the unit cell (purple) back to the original monomer. Figure 5 highlights how B86bPBE-XDM dramatically overestimates the photodimerization and dissociation energies, which is corrected by combining the periodic DFT energies with intramolecular SCS-MP2D. Finally, the intramolecular dispersion correction in SCS-MP2D is key to describing the photodimer; the MP2 (and MP2C) errors are several-fold larger. ¹

5 Outlook

In summary, dispersion-corrected MP2 models provide a reliable and cost-effective approach that can readily be applied to organic species with more than 100 atoms. For organic conformational energies and non-covalent interactions, the accuracy of SCS-MP2D is superior to conventional GGA and hybrid density

functionals, and it is often similar to or better than that of functionals such as ω B97M-V or earlier-generation double-hybrid functionals. Several molecular crystal examples were presented in which SCS-MP2D was successfully used to address the intramolecular delocalization error present in the periodic DFT treatment. Though not discussed here, the MP2D models have also been applied to intermolecular interactions in crystals, ^{36,41} and it could provide an alternative to DFT for parameterizing tailor-made force fields.

Moving forward, the SCS-MP2D method should be extended to a wider array of maingroup elements (but not transition metals, for which single-reference HF often performs poorly). This extension should be straightforward, as the necessary dispersion coefficients can be computed readily. Beyond that, there are several open questions. Could the accuracy of SCS-MP2D be improved considerably by parameterizing it against a much larger set of training data? That approach led to significant improvements between DSD-PBEP86-D3(BJ) and revDSD-PBEP86-D3(BJ). How could the dispersion treatment be improved further? Switching from D3 to D4 would allow the coefficients to adapt better to charge states, for example. Still, the local coordination descriptors used by D3 and D4 to interpolate the dispersion coefficients cannot capture nuances such as how the dispersion coefficients change in large polyaromatic hydrocarbons, for example. Finally, more testing is needed to understand how SCS-MP2D behaves for reaction thermochemistry and open-shell systems.

6 Acknowledgments

G.J.O.B. gratefully acknowledges support for this work from the National Science Foundation (CHE-1955554) and supercomputer time from ACCESS (CHE110064). J.Ř. acknowledges the support from the Ministry of Education, Youth and Sports of the Czech Republic through the e-INFRA CZ (ID:90254).

Biographies

- Gregory Beran earned his Ph.D at the University of California Berkeley in 2005, working with Prof. Martin Head-Gordon, and performed postdoctoral research with Prof. William H. Green at the Massachusetts Institute of Technology. Since 2007, he has been a professor at the University of California Riverside, with research interests focusing on the development and application of electronic structure methods for non-covalent interactions and organic crystal structure prediction.
- Chandler Greenwell is a Business Development Manager and Solid State Applications Scientist at XtalPi. He earned his Ph.D at the University of California, Riverside in 2020, working with Prof. Gregory Beran. He is focused on increasing the synergy between computational and experimental methods in industrial material science research. He works with pharmaceutical companies to implement crystal structure prediction into their solid state work flows.
- Cameron Cook is a postdoctoral researcher at Bristol Myers Squibb. He earned his Ph.D at the University of California, Riverside in 2022, working with Prof. Gregory Beran. His research interests include model development for finite temperature contributions to organic molecular crystal free energies, and computational strategies for predicting mechanical properties of photomechanical materials. Recently, Dr. Cook has been using crystal structure prediction techniques for pharmaceutical product development.
- Jan Řezáč is a senior researcher at Institute of Organic Chemistry and Biochemistry, Academy of Sciences of the Czech Republic. He obtained his PhD at Charles University in Prague in 2008, working with Prof. P. Hobza. Then, he

spent his postdoctoral study with Prof. D. R. Salahub at the University of Calgary, Canada. Dr Řezáč's main research interests are benchmark calculations of non-covalent interactions, development of semiempirical QM methods and their application to biomolecular systems.

References

- 1 Greenwell, C.; Řezáč, J.; Beran, G. J. O. Spin-component-scaled and dispersion-corrected second-order Møller-Plesset perturbation theory: An alternative path toward chemical accuracy. *Phys. Chem. Chem. Phys.* **2022**, *24*, 3695–3712.
- 2 Greenwell, C.; Beran, G. J. O. Inaccurate conformational energies still hinder crystal structure prediction in flexible organic molecules. *Cryst. Growth Des.* **2020**, *20*, 4875–4881.
- 3 Beran, G. J. O.; Sugden, I. J.; Greenwell, C.; Bowskill, D. H.; Pantelides, C. C.; Adjiman, C. S. How many more polymorphs of ROY remain undiscovered? *Chem. Sci.* **2022**, *13*, 1288–1297.
- 4 Cook, C. J.; Li, W.; Lui, B. F.; Gately, T. J.; Al-Kaysi, R. O.; Mueller, L. J.; Bardeen, C. J.; Beran, G. J. O. A theoretical framework for the design of photomechanical engines. *Chem. Sci.* **2022**, 14, 937–949.
- 5 Grimme, S.; Hansen, A.; Brandenburg, J. G.; Bannwarth, C. Dispersion-Corrected Mean-Field Electronic Structure Methods. *Chem. Rev.* **2016**, *116*, 5105–5154.
- 6 Mardirossian, N.; Head-Gordon, M. Thirty years of density functional theory in computational chemistry: An overview and extensive assessment of 200 density functionals. *Molec. Phys.* **2017**, *115*, 2315–2372.
- 7 Martin, J. M. L.; Santra, G. Empirical Double-Hybrid Density Functional Theory:

- A 'Third Way' in Between WFT and DFT. *Israel J. Chem.* **2020**, *60*, 787–804.
- 8 Grimme, S. Improved second-order Møller–Plesset perturbation theory by separate scaling of parallel- and antiparallel-spin pair correlation energies. *J. Chem. Phys.* **2003**, *118*, 9095.
- 9 Hesselmann, A. Improved supermolecular second order Møller-Plesset intermolecular interaction energies using time-dependent density functional response theory. *J. Chem. Phys.* **2008**, *128*, 144112.
- 10 Pitonak, M.; Hesselmann, A. Accurate Intermolecular Interaction Energies from a Combination of MP2 and TDDFT Response Theory. J. Chem. Theory Comput. 2010, 6, 168–178.
- 11 Tkatchenko, A.; DiStasio, R. A.; Head-Gordon, M.; Scheffler, M. Dispersion-corrected Møller-Plesset second-order perturbation theory. J. Chem. Phys. 2009, 131, 094106.
- 12 Huang, Y.; Beran, G. J. O. Reliable prediction of three-body intermolecular interactions using dispersion-corrected second-order Møller-Plesset perturbation theory. J. Chem. Phys. 2015, 143, 044113.
- 13 Řezáč, J.; Greenwell, C.; Beran, G. J. O. Accurate non-covalent interactions via dispersion-corrected second-order Møller-Plesset perturbation theory. J. Chem. Theory Comput. 2018, 14, 4711–4721.
- 14 Lochan, R. C.; Head-Gordon, M. Orbital-optimized opposite-spin scaled second-order correlation: An economical method to improve the description of open-shell molecules. *The Journal of Chemical Physics* **2007**, *126*.
- 15 Bozkaya, U.; Turney, J. M.; Yamaguchi, Y.; Schaefer, H. F.; Sherrill, C. D. Quadratically convergent algorithm for orbital optimization in the orbital-optimized coupled-cluster doubles method and in orbital-optimized second-order Møller-Plesset per-

- turbation theory. The Journal of Chemical Physics 2011, 135.
- 16 Goldey, M.; Head-Gordon, M. Attenuating Away the Errors in Inter- and Intramolecular Interactions from Second-Order Møller–Plesset Calculations in the Small Aug-cc-pVDZ Basis Set. J. Phys. Chem. Lett. 2012, 3, 3592–3598.
- 17 Huang, Y.; Goldey, M.; Head-Gordon, M.; Beran, G. J. O. Achieving high-accuracy intermolecular interactions by combining Coulomb-attenuated second-order Møller-Plesset perturbation theory with coupled Kohn-Sham dispersion. J. Chem. Theory Comput. 2014, 10, 2054–2063.
- 18 Shee, J.; Loipersberger, M.; Rettig, A.; Lee, J.; Head-Gordon, M. Regularized Second-Order Møller-Plesset Theory: A More Accurate Alternative to Conventional MP2 for Noncovalent Interactions and Transition Metal Thermochemistry for the Same Computational Cost. J. Phys. Chem. Lett. 2021, 12, 12084–12097.
- 19 Sedlak, R.; Riley, K. E.; Řezáč, J.; Pitoňák, M.; Hobza, P. MP2.5 and MP2.X: approaching CCSD(T) quality description of noncovalent interaction at the cost of a single CCSD iteration. *ChemPhysChem* **2013**, *14*, 698–707.
- 20 Řezáč, J. Non-Covalent Interactions Atlas benchmark data sets 5: London dispersion in an extended chemical space. *Phys. Chem. Chem. Phys.* **2022**, *24*, 14780–14793.
- 21 Chalasinski, G.; Szczesniak, M. M. On the connection between the supermolecular Møller-Plesset treatment of the interaction energy and the perturbation theory of intermolecular forces. *Mol. Phys.* 1988, 63, 205– 224.
- 22 Cybulski, S. M.; Chalasinski, G.; Moszynski, R. On decomposition of second-order Møller-Plesset supermolecular interaction energy and basis set effects. *J. Chem. Phys.* **1990**, *92*, 4357–4363.

- 23 Cybulski, S. M.; Lytle, M. L. The origin of deficiency of the supermolecule second-order Møller-Plesset approach for evaluating interaction energies. *J. Chem. Phys.* **2007**, 127, 141102.
- 24 Burns, L. A.; Marshall, M. S.; Sherrill, C. D. Appointing silver and bronze standards for noncovalent interactions: A comparison of spin-component-scaled (SCS), explicitly correlated (F12), and specialized wavefunction approaches. J. Chem. Phys. 2014, 141, 234111.
- 25 Grimme, S.; Antony, J.; Ehrlich, S.; Krieg, H. A consistent and accurate ab initio parametrization of density functional dispersion correction (DFT-D) for the 94 elements H-Pu. J. Chem. Phys. **2010**, 132, 154104.
- 26 Rezáč, J.; Riley, K. E.; Hobza, P. S66: A Well-Balanced Database of Benchmark Interaction Energies Relevant to Biomolecular Structures. J. Chem. Theory Comput. 2011, 7, 2427–2438.
- 27 Grimme, S.; Goerigk, L.; Fink, R. F. Spin-component-scaled electron correlation methods. WIRES: Comput. Mol. Sci. 2012, 2, 886–906.
- 28 Distasio, R. A.; Head-Gordon, M. Optimized spin-component scaled second-order Møller-Plesset perturbation theory for intermolecular interaction energies. *Mol. Phys.* 2007, 105, 1073–1083.
- 29 Smith, D. G. A.; Burns, L. A.; Simmonett, A. C.; Parrish, R. M.; Schieber, M. C.; Galvelis, R.; Kraus, P.; Kruse, H.; Di Remigio, R.; Alenaizan, A.; James, A. M.; Lehtola, S.; Misiewicz, J. P.; Scheurer, M.; Shaw, R. A.; Schriber, J. B.; Xie, Y.; Glick, Z. L.; Sirianni, D. A.; O'Brien, J. S.; Waldrop, J. M.; Kumar, A.; Hohenstein, E. G.; Pritchard, B. P.; Brooks, B. R.; Schaefer, Η. F.; Sokolov, Α. Y.; DePrince, Patkowski, K.: Α. E.; Bozkaya, U.; King, R. A.; Evangelista, F. A.; Turney, J. M.; Crawford, T. D.;

- Sherrill, C. D. PSI4 1.4: Open-source software for high-throughput quantum chemistry. *J. Chem. Phys.* **2020**, *152*, 184108.
- 30 The MP2D software can be downloaded at https://github.com/Chandemonium/MP2D.
- 31 Řezáč, J. Cuby: An integrative framework for computational chemistry. *J. Comp. Chem.* **2016**, *37*, 1230–1237.
- 32 Santra, G.; Sylvetsky, N.; Martin, J. M. L. Minimally Empirical Double-Hybrid Functionals Trained against the GMTKN55 Database: revDSD-PBEP86-D4, revDOD-PBE-D4, and DOD-SCAN-D4. *J. Phys. Chem. A* **2019**, *123*, 5129–5143.
- 33 Santra, G.; Martin, J. M. L. Does GLPT2 offer any actual benefit over conventional HF-MP2 in the context of double-hybrid density functionals? 2022; p 020015.
- 34 Burns, L. A.; Faver, J. C.; Zheng, Z.; Marshall, M. S.; Smith, D. G. A.; Vanommeslaeghe, K.; MacKerell, A. D.; Merz, K. M.; Sherrill, C. D. The BioFragment Database (BFDb): An open-data platform for computational chemistry analysis of noncovalent interactions. J. Chem. Phys. 2017, 147, 161727.
- 35 Goerigk, L.; Hansen, A.; Bauer, C.; Ehrlich, S.; Najibi, A.; Grimme, S. A look at the density functional theory zoo with the advanced GMTKN55 database for general main group thermochemistry, kinetics and noncovalent interactions. *Phys. Chem. Chem. Phys.* **2017**, *19*, 32184–32215.
- 36 Beran, G. J. O.; Wright, S. E.; Greenwell, C.; Cruz-Cabeza, A. J. The interplay of intra- and intermolecular errors in modeling conformational polymorphs. *J. Chem. Phys.* **2022**, *156*, 104112.
- 37 Řezáč, J. Non-Covalent Interactions Atlas Benchmark Data Sets: Hydrogen Bonding. *J. Chem. Theory Comput.* **2020**, *16*, 2355–2368.

- 38 Řezáč, J. Non-Covalent Interactions Atlas Benchmark Data Sets 2: Hydrogen Bonding in an Extended Chemical Space. *J. Chem. Theory Comput.* **2020**, *16*, 6305–6316.
- 39 Kříž, K.; Nováček, M.; Řezáč, J. Non-Covalent Interactions Atlas Benchmark Data Sets 3: Repulsive Contacts. *Journal of Chemical Theory and Computation* **2021**, 17, 1548–1561.
- 40 Kříž, K.; Řezáč, J. Non-covalent interactions atlas benchmark data sets 4: σ-hole interactions. *Phys. Chem. Chem. Phys.* **2022**, 24, 14794–14804.
- 41 Greenwell, C.; McKinley, J. L.; Zhang, P.; Zeng, Q.; Sun, G.; Li, B.; Wen, S.; Beran, G. J. O. Overcoming the difficulties of predicting conformational polymorph energetics in molecular crystals via correlated wavefunction methods. *Chem. Sci.* **2020**, *11*, 2200–2214.
- 42 Raghavachari, K.; Saha, A. Accurate Composite and Fragment-Based Quantum Chemical Models for Large Molecules. *Chem. Rev.* **2015**, *115*, 5643–5677.
- 43 Wen, S.; Nanda, K.; Huang, Y.; Beran, G. J. O. Practical quantum mechanics-based fragment methods for predicting molecular crystal properties. *Phys. Chem. Chem. Phys.* **2012**, *14*, 7578–7590.
- 44 Wen, S.; Beran, G. J. O. Accidental degeneracy in crystalline aspirin: New insights from high-level ab initio calculations. *Cryst. Growth Des.* **2012**, *12*, 2169–2172.
- 45 Wen, S.; Beran, G. J. O. Crystal polymorphism in oxalyl dihydrazide: Is empirical DFT-D accurate enough? *J. Chem. Theory Comput.* **2012**, *8*, 2698–2705.
- 46 Červinka, C.; Beran, G. J. O. Ab initio prediction of the polymorph phase diagram for crystalline methanol. *Chem. Sci.* **2018**, *9*, 4622–4629.

- 47 Nanda, K.; Beran, G. J. O. What governs the proton-ordering in ice XV? *J. Phys. Chem. Lett.* **2013**, *4*, 3165–3169.
- 48 Sontising, W.; Heit, Y. N.; McKinley, J. L.; Beran, G. J. O. Theoretical predictions suggest carbon dioxide phases III and VII are identical. *Chem. Sci.* **2017**, *8*, 7374–7382.
- 49 Sontising, W.; Beran, G. J. O. Theoretical assessment of the structure and stability of the λ phase of nitrogen. *Phys. Rev. Mater.* **2019**, *3*, 095002.
- 50 Sontising, W.; Beran, G. J. O. Combining crystal structure prediction and simulated spectroscopy in pursuit of the unknown nitrogen phase ζ crystal structure. *Phys. Rev. Mater* **2020**, 4, 063601.
- 51 Hirata, S.; Gilliard, K.; He, X.; Li, J.; Sode, O. Ab initio molecular crystal structures, spectra, and phase diagrams. *Acc. Chem. Res.* **2014**, *47*, 2721–30.
- 52 Červinka, C.; Fulem, M. Cohesive properties of the crystalline phases of twenty proteinogenic α-aminoacids from first-principles calculations. *Phys. Chem. Chem. Phys.* **2019**, 21, 18501–18515.
- 53 Červinka, C.; Fulem, M. Probing the Accuracy of First-Principles Modeling of Molecular Crystals: Calculation of Sublimation Pressures. *Crystal Growth and Design* **2019**, *19*, 808–820.
- 54 Greenwell, C.; Beran, G. J. O. Rubrene untwisted: common density functional theory calculations overestimate its deviant tendencies. *J. Mater. Chem. C* **2021**, *9*, 2848–2857.
- 55 Chekal, B. P.; Campeta, A. M.; Abramov, Y. A.; Feeder, N.; Glynn, P. P.; McLaughlin, R. W.; Meenan, P. A.; Singer, R. A. The Challenges of Developing an API Crystallization Process for a Complex Polymorphic and Highly Solvating System. Part I. Org. Proc. Res. Dev. 2009, 13, 1327–1337.

- 56 Campeta, A. M.; Chekal, B. P.; Abramov, Y. A.; Meenan, P. A.; Henson, M. J.; Shi, B.; Singer, R. A.; Horspool, K. R. Development of a Targeted Polymorph Screening Approach for a Complex Polymorphic and Highly Solvating API. J. Pharm. Sci. 2010, 99, 3874–3886.
- 57 Lupyan, D.; Abramov, Y. A.; Sherman, W. Close intramolecular sulfur-oxygen contacts: Modified force field parameters for improved conformation generation. *J. Comput. Aided Mol. Des.* **2012**, *26*, 1195–1205.
- 58 Vasileiadis, M.; Pantelides, C. C.; Adjiman, C. S. Prediction of the crystal structures of axitinib, a polymorphic pharmaceutical molecule. *Chem. Eng. Sci.* **2015**, *121*, 60–76.
- 59 Yu, L. Polymorphism in Molecular Solids: An Extraordinary System of Red, Orange, and Yellow Crystals. *Acc. Chem. Res.* **2010**, 43, 1257–1266.
- 60 Li, X.; Ou, X.; Rong, H.; Huang, S.; Nyman, J.; Yu, L.; Lu, M. The Twelfth Solved Structure of ROY: Single Crystals of Y04 Grown from Melt Microdroplets. *Cryst. Growth Des.* **2020**, *20*, 7093–7097.
- 61 Nyman, J.; Yu, L.; Reutzel-Edens, S. M. Accuracy and reproducibility in crystal structure prediction: the curious case of ROY. CrystEngComm 2019, 21, 2080–2088.
- 62 Vasileiadis, M.; Kazantsev, A. V.; Karamertzanis, P. G.; Adjiman, C. S.; Pantelides, C. C. The polymorphs of ROY: application of a systematic crystal structure prediction technique. *Acta Cryst. B* **2012**, *68*, 677–685.
- 63 Lévesque, A.; Maris, T.; Wuest, J. D. ROY Reclaims Its Crown: New Ways to Increase Polymorphic Diversity. *J. Am. Chem. Soc.* **2020**, *142*, 11873–11883.
- 64 Tan, M.; Shtukenberg, A. G.; Zhu, S.; Xu, W.; Dooryhee, E.; Nichols, S. M.;

- Ward, M. D.; Kahr, B.; Zhu, Q. ROY revisited, again: the eighth solved structure. *Faraday Disc.* **2018**, *211*, 477–491.
- 65 Feng, X.; Becke, A. D.; Johnson, E. R. Theoretical investigation of polymorph- and coformer-dependent photoluminescence in molecular crystals. *CrystEngComm* **2021**, 23, 4264–4271.
- 66 Thomas, S. P.; Spackman, M. A. The Polymorphs of ROY: A Computational Study of Lattice Energies and Conformational Energy Differences. Austral. J. Chem. 2018, 71, 279.
- 67 Awad, W. M.; Davies, D. W.; Kitagawa, D.; Mahmoud Halabi, J.; Al-Handawi, M. B.; Tahir, I.; Tong, F.; Campillo-Alvarado, G.; Shtukenberg, A. G.; Alkhidir, T.; Hagiwara, Y.; Almehairbi, M.; Lan, L.; Hasebe, S.; Karothu, D. P.; Mohamed, S.; Koshima, H.; Kobatake, S.; Diao, Y.; Chandrasekar, R.; Zhang, H.; Sun, C. C.; Bardeen, C.; Al-Kaysi, R. O.; Kahr, B.; Naumov, P. Mechanical properties and peculiarities of molecular crystals. *Chem. Soc. Rev.* 2023, *52*, 3098–3169.
- 68 Chalek, K. R.; Dong, X.; Tong, F.; Kudla, R. A.; Zhu, L.; Gill, A. D.; Xu, W.; Yan, C.; Hartman, J. D.; Magalhaes, A.; Al-Kaysi, R. O.; Hayward, R. C.; Hooley, R. J.; Beran, G. J. O.; Bardeen, C. J.; Mueller, L. J. Bridging photochemistry and photomechanics with NMR crystallography: the molecular basis for the macroscopic expansion of an anthracene ester nanorod. *Chem. Sci.* **2021**, *12*, 453–463.
- 69 Zhu, L.; Al-Kaysi, R. O.; Bardeen, C. J. Reversible Photoinduced Twisting of Molecular Crystal Microribbons. *J. Am. Chem. Soc.* **2011**, *133*, 12569–12575.
- 70 Yang, C.; Zhu, L.; Kudla, R. A.; Hartman, J. D.; Al-Kaysi, R. O.; Monaco, S.; Schatschneider, B.; Magalhaes, A.; Beran, G. J. O.; Bardeen, C. J.; Mueller, L. J. Crystal structure of the meta-stable intermediate in the photomechanical, crystal-to-

- crystal reaction of 9-tertbutyl anthracene ester. CrystEngComm 2016, 18, 7319–7329.
- 71 Beran, G. J. O. First-principles computations indicate that solid state photodimerization of 9-tert-butyl anthracene ester produces an exceptionally metastable polymorph. CrystEngComm 2019, 21, 758–764.
- 72 Gately, T. J.; Sontising, W.; Easley, C. J.; Islam, I.; Al-Kaysi, R. O.; Beran, G. J. O.; Bardeen, C. J. Effect of halogen substitution on energies and dynamics of reversible photomechanical crystals based on 9-anthracenecarboxylic acid. CrystEng-Comm 2021, 23, 5931–5943.
- 73 Cook, C. J.; Perry, C. J.; Beran, G. J. O. Organic crystal packing is key to determining the photomechanical response. *J. Phys. Chem. Lett.* **2023**, *14*, 6823–6831.
- 74 Perry, C. J.; Beran, G. J. O. Understanding the impact of halogenation on the crystalline photomechanical response properties of 9-anthracene carboxylic acid from first-principles. Cryst. Growth Des. 2023, submitted.
- 75 Grimme, S.; Diedrich, C.; Korth, M. The Importance of Inter- and Intramolecular van der Waals Interactions in Organic Reactions: the Dimerization of Anthracene Revisited. *Angew. Chem. Int. Ed.* **2006**, *45*, 625–629.

TOC Graphic

